

Detonation model using Burgers equation and a pulsed reaction

S. SM. Lau-Chapdelaine and M. I. Radulescu
 Department of Mechanical Engineering, University of Ottawa
 Ottawa, Ontario, Canada

1 Introduction

Detonations are unstable, exhibiting a pulsating or galloping behaviour in one dimension. The instability is observed experimentally in narrow tubes close to the detonation limit [1], characterized by periodic and abrupt accelerations of the detonation in excess of the Chapman-Jouguet speed [2], followed by a long decay to nearly half of the Chapman-Jouguet detonation velocity. This behaviour is not unique to near-limit conditions, but occurs over a large range of conditions. Simulations of the Euler equations with simplified chemistry [3, 4] have shown that oscillations in detonation speed may undergo period-doubling as the activation energy is increased, eventually becoming chaotic. This period-doubling route to chaos also occurs in systems with simplified detonation dynamics involving Burgers equation [5, 6].

Limit cycles of period-two oscillations are shown in figure 1 for detonations in the Euler equations and two simplified models. These phase diagrams have two distinct decay rates highlighted in red and blue, separated by re-amplifications. These two decay time scales seem to be intrinsic to the first period-doubling bifurcation and appear to persist through further period-doubling bifurcations and onto chaos.

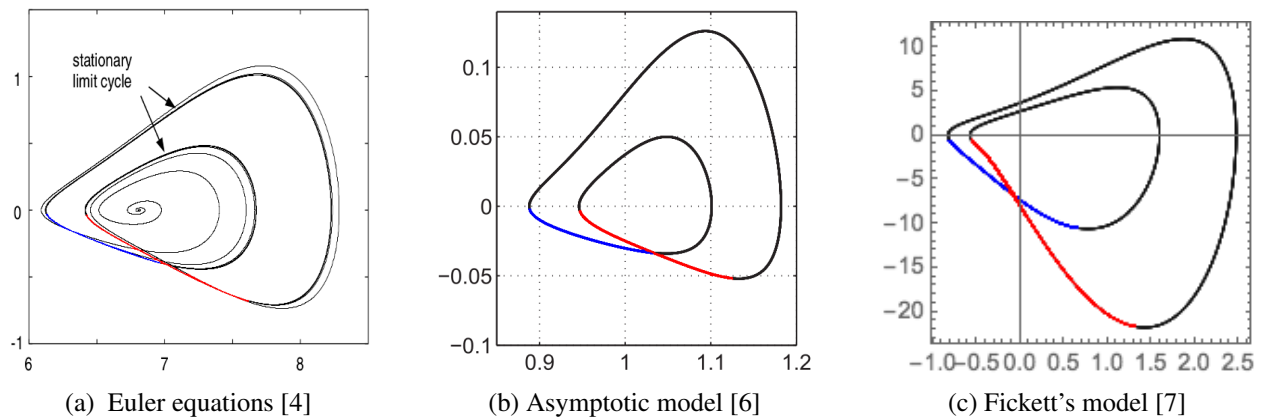


Figure 1: Phase diagrams of dD/dt as functions of D for period-two bifurcations in three detonation models, with two decay rates highlighted in red and blue

Motivated by the period-doubling bifurcation route to chaos, this paper introduces a simplified model to study the two distinct decay rates. Burgers equation will be used to simplify the hydrodynamics, and the fast dynamics of re-amplification will be replaced by simple pulsations. A similar model was first introduced by Radulescu and Shepherd [8] for the reactive Euler equations.

2 Model

The hydrodynamic equation can be asymptotically derived [9–11] from the Navier-Stokes equations in the Newtonian limit with weak heat release, yielding Burgers equation with a source term

$$\frac{\partial u}{\partial t} + \frac{1}{2} \frac{\partial}{\partial x} (u^2 + \lambda q) = 0$$

where u is the local information speed, t is time, and x is location. The hydrodynamics are coupled to a source term $q\lambda$ to account for reactions. The constant $q = 1$ is the heat released by combustion and $\lambda = 0$ when unburnt, or $\lambda = 1$ when burnt. Reactions are forced at fixed time intervals $t_p = 1$, independent of the hydrodynamics. At each interval, all shocked reactants are consumed completely and simultaneously, i.e. $\lambda = 1 \forall x \leq x_s$ when $t \bmod t_p = 0$. No reactions occur in the mean time and the interface between burnt and unburnt gasses remains still in the model's frame of reference. The pulsed reaction greatly simplifies the complicated dynamics of re-amplification. Using Burgers equation also simplifies the characteristics, leaving only forward-travelling characteristics to be considered, moving at the local speed u .

3 Numerical Method

Simulations were performed in the lab and shock frames of reference with negligible differences between the two. The shock frame simulations were used for all results, with exception of figure 5. The flow field was initiated by an under-driven piston where $u = 0.5$ behind the shock, $u = 0$ elsewhere, and $\lambda = 0$ everywhere.

In the shock frame simulations, the post-shock state was used as boundary condition on the right side, and the zero-gradient condition was used on the left side. A uniform grid of 4000 points per $D_{CJ}t_p$ covered the domain. Increasing the resolution increased the sharpness of discontinuities, but had no qualitative effect.

The Riemann problem was solved at every cell interface using a first-order Godunov method [12] with a first-order Euler method in time. The time step size was the minimum between the time step dictated by the Courants-Freidrich-Lewy condition and the time to the next scheduled pulse

$$\Delta t = \min \left(\text{CFL} \times \frac{\Delta x}{u_{\max}}, t_p - t \bmod t_p \right)$$

adjusted appropriately in the shock-frame of reference and with $\text{CFL} = 0.5$.

4 Results

The time evolution of the shock front speed is plotted in figure 2 and profiles of u and reaction zone location are shown in figure 3, for the initiation transient, and for the fully developed pulsations in figure 4.

Initial conditions of $u = 0.5$ are maintained until the first pulse when the reaction front jumps to the front. The shock travels away from the reaction zone at constant speed, unattenuated, while another discontinuity in u remains with the reaction front as seen in figure 3a. The second pulse occurs, bringing the reaction front to the shock front. The shock speed is immediately increased, and the shock travels away from the new reaction front. An expansion wave is created at the reaction zone's previous location, and the head of this expansion fan (the fastest portion of the rarefaction) travels towards the shock front, circled in figure 3b.

The rarefaction passes through the reaction discontinuity, seen in figure 3c, reaching the shock just before the third pulse, shown in figure 3d. The third pulse resets the reaction zone at front and increases the shock speed. The shock immediately begins decaying, while a new expansion fan forms at the reaction zone's pre-pulse position, shown in figure 3e. The head of the new rarefaction (circled in figures 3d and 3e) travels behind the previous expansion, joined at a kink around $x - x_s \approx -0.7$ at $t = 3.3$. The kink, along with the rest of the rarefaction, travels through the reaction zone towards the shock and reaches the front following the fourth pulse. The ensuing pulses behave similarly, becoming fully developed around the tenth pulse.

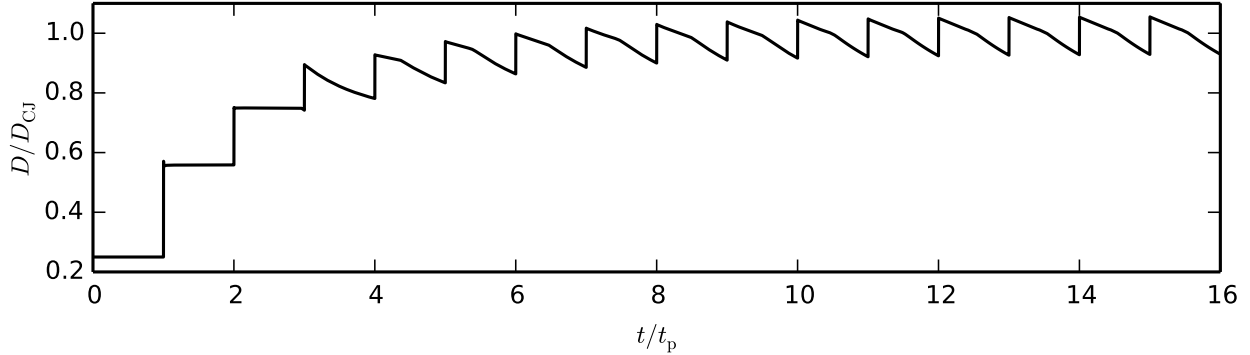
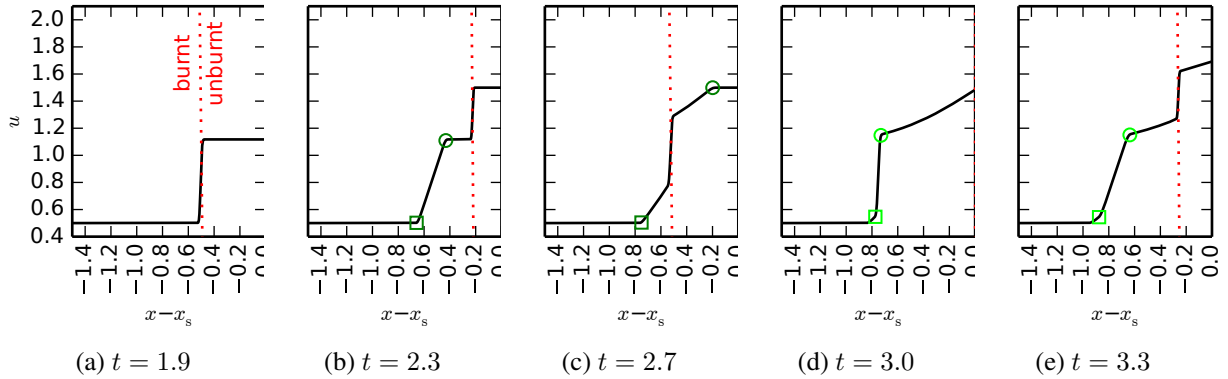


Figure 2: Detonation speed evolution

Figure 3: Profiles of u (solid) during initial cycles with the burnt-unburnt interface (dotted), expansion fan head (circle) and expansion fan tail (square)

The regular cycle is shown in figure 4. It starts with the reaction zone at the front where the pulse amplifies the shock. A strong expansion fan is created at $x - x_s \approx -1$ where the discontinuity in the flow is no longer supported by the reaction front. The kink indicated by the dashed circle corresponds to the expansion fan head from the previous cycle. The reaction zone falls behind while the freshly amplified shock begins to decay. The head from the previous cycle reaches the front after $t = 14.4$ and the new expansion head (solid circle) moves forward. The head from the current cycle passes through the reaction zone after $t = 14.6$.

5 Analysis

Numerical simulations revealed a sawtooth evolution of the detonation front velocity, shown in figure 2, with a period-averaged speed equal to the Chapman-Jouguet detonation velocity, also found by Mi and Higgins

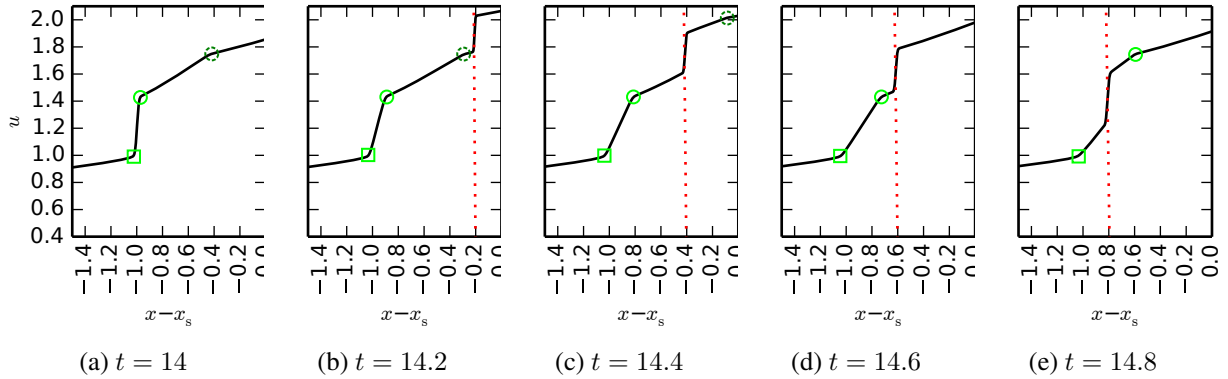


Figure 4: Profiles of u (solid) over one regular cycle with the burnt-unburnt interface (dotted), expansion fan heads from current (solid circle) and previous (dashed circle) cycles, and expansion fan tail (square)

[13] in a similar system. However, here the detonation velocity decay is composed of two sequential distinct rates, seen in figure 2, punctuated by reaction pulses. The shock speed decay is caused by expansion waves at the shock front, generated in the rear when the reaction zone jumps to the front. The discontinuity in decay rate occurs when the head of the expansion from the previous pulse arrives at the front.

The flow can also be visualized by looking at a characteristic diagram, shown in figure 5 once the detonation has adopted its regular oscillatory behaviour. The characteristics are plotted in a steady frame of reference travelling at D_{CJ} with the origin situated at the shock front immediately after a pulse. In this frame of reference, the characteristics have slopes of $1/(u - D_{CJ})$. Characteristics which travel at a speed $u \leq D_{CJ}$, where $x - D_{CJ}t < -1$, and the limiting characteristic (vertical, $u = D_{CJ}$) will never reach the shock front, whereas characteristics to the right of the limiting characteristic eventually reach the front. The reaction zone position is plotted in red and characteristics ahead of the shock are omitted for clarity.

The expansion fan created at the beginning of each pulse can be seen in figure 5 between the limiting characteristic and the characteristic highlighted in green between $t = 0$ and $t = 1$. The green characteristic represents the head of the rarefaction, the fastest characteristic in the expansion fan. The characteristics amplify and accelerate when they cross the reaction zone, shown by their change in slope as they cross the reaction zone. Nearly vertical characteristics emanating from the tail (the slowest portion of the expansion fan coming from the squares in figure 4), are amplified just before the pulse at $t = 1$ and lie next to the head (green) characteristic from the new pulse. Characteristics from the original pulse are amplified a second time as they pass through the reaction zone from the second pulse. The head characteristic reaches the shock front slightly after $t = 1.5$. However, not all of the characteristics from the original rarefaction reach the front before the next pulse. The last characteristic that reaches the front before the third pulse is highlighted in blue. All characteristics above the blue characteristic are amplified a third time by the reaction zone before reaching the shock, over two periods after they were released.

Characteristics that are only amplified twice decay faster than those which are amplified three times which manifests into the two distinct hydrodynamic decay rates of the lead shock speed seen in figure 2. This time scale separation of forward-facing pressure waves may be responsible for the period-doubling behaviour of detonations.

The strength of the characteristics, times, and locations of their amplifications can be found analytically.

The Rankine-Hugoniot jump condition for a discontinuity is

$$S = \frac{[\frac{1}{2}u^2 + \frac{1}{2}q\lambda]}{[u]} = \frac{(\frac{1}{2}u_r^2 + \frac{1}{2}q\lambda_r) - (\frac{1}{2}u_l^2 + \frac{1}{2}q\lambda_l)}{(u_r - u_l)} \quad (1)$$

with discontinuity speed S . The equation simplifies, for the immobile ($S = 0$) reaction zone where flow is reacted on the left ($\lambda_l = 1$) and unreacted on the right ($\lambda_r = 0$), to $u_r = \sqrt{u_l^2 + q}$, allowing the amplification of a characteristic across the reaction zone to be quantified. Conditions for the analysis of a pulsation are taken from the characteristics diagram in figure 5 which indicates that the limiting characteristic travels at $u = D_{CJ}$, the average detonation speed is $D_{CJ} = \sqrt{q}$, and that an expansion fan is created at each pulse. This means the expansion fan created at each pulse ranges from $u = D_{CJ}$ at the tail of the fan where the limiting characteristic is unamplified, to $u = \sqrt{D_{CJ}^2 + q}$ at the head where it is most amplified. The strength of intermediate characteristics in the expansion fan is given by $u = x/t$, centred about the last position of the reaction zone before a pulse. The strength u of any characteristic originating at any pulse is therefore known as functions of (x, t) . The time and location of its next amplification is calculated simply by finding the intersection between the characteristic and reaction zone, which are both straight line segments. The speed of the amplified characteristic is then calculated with the Rankine-Hugoniot jump across the reaction zone, and the next amplification point can be located using the same procedure. This allows u to be calculated at any point (x, t) to the right of the limiting characteristic.

For example, this procedure can be used to find the blue characteristic of figure 5 which arrives at the shock when a pulse occurs, $x - D_{CJ}t = 0$, and two pulses after its creation. The strength u_s of the blue characteristic at the shock, amplified twice, can be solved numerically from

$$t = 2t_p = \frac{u_s D_{CJ} t_p}{u_s - D_{CJ}} \left(\frac{1}{\sqrt{u_s^2 - 2q}} + \frac{1}{\sqrt{u_s^2 - q}} - \frac{1}{u_s} \right) \quad (2)$$

to yield the minimum shock strength of $u_s = 1.86$. Amplifying this characteristic a third time gives $u_s = 2.11$, the maximum shock strength which occurs immediately after a pulse. The shock speed can be calculated from the Rankine-Hugoniot relation (equation 1) for a shock propagating into $u = 0$, yielding $D = u_s/2$. The strength of the blue characteristic agrees well with the value obtained from the slope of the characteristic diagram in figure 5. This process can also be used to estimate the time at which the head and tail characteristics reach the shock front, $t \approx 1.57t_p$ and $t \approx 2.57t_p$ respectively, following their creation.

6 Conclusion

A simplified pulsating detonation model was studied using the Fickett-Majda asymptotic model for detonations in the limit of small heat release and the Newtonian limit, with a periodic reaction which consumed all shocked gas. It was used to study the decay behaviour of pulsating detonations. The detonation was found to travel at a pulse-averaged speed equal to the Chapman-Jouguet velocity. Two distinct decay rates of the shock speed were found per cycle, a feature present in period-two detonations.

After each pulse, a strong expansion wave was created at the last location of reaction interface. A characteristic investigation revealed that characteristics originating from the head of this expansion took approximately one-and-a-half periods to reach and attenuate the detonation front, while characteristics from the tail took an additional period. The leading characteristics were amplified twice by passing through subsequent reaction interfaces, before arriving at the front, whilst the weaker trailing characteristics were amplified three times. These dynamics produced the humped profile with two decay rates. These two decay rates intrinsic to pulsating detonations may be the source of period-doubling bifurcations which lead to chaos.

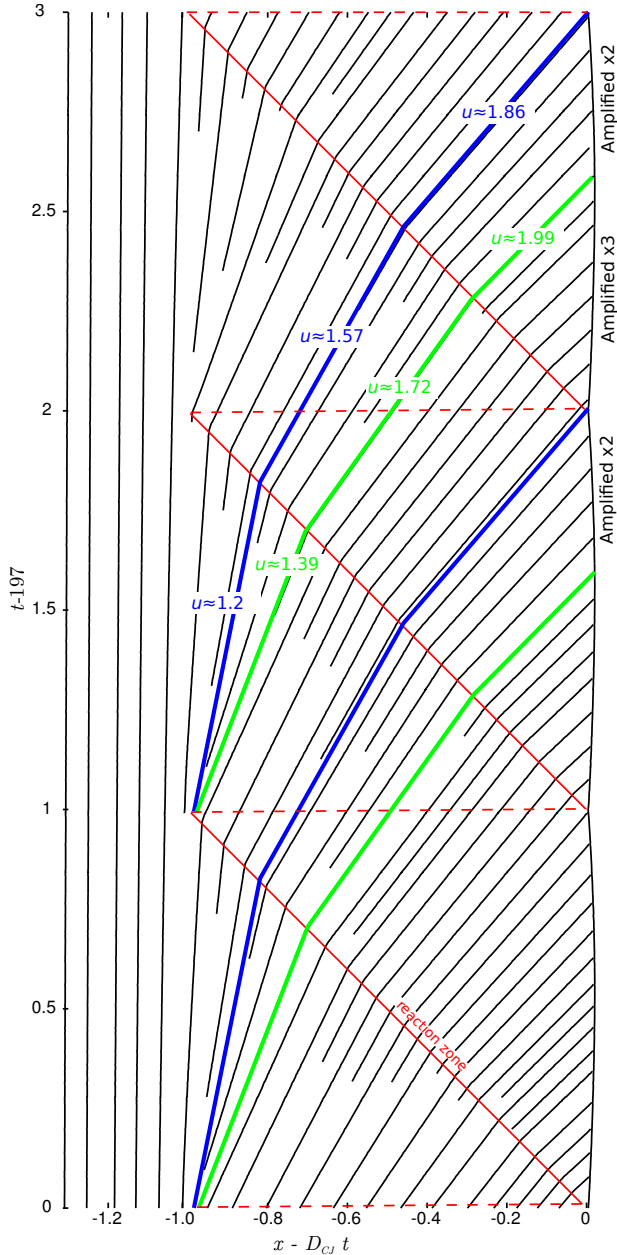


Figure 5: Characteristics diagram (black) and reaction zone position (red) over three periods, after the detonation has reached its regular pulsating behaviour ($t = 197$ to 200 , abscissa shifted so $x - D_{CJ} = 0$ coincides with shock position at pulse); blue and green characteristics delimit characteristics amplified twice from those amplified three times

References

- [1] J. H. S. Lee, *The detonation phenomenon*. Cambridge: Cambridge University Press, 2008.
- [2] S. Jackson, B. J. Lee, and J. E. Shepherd, "Detonation mode and frequency analysis under high loss conditions for stoichiometric propane-oxygen," *Combustion and Flame*, vol. 167, pp. 24–38, 2016.
- [3] H. Ng, A. Higgins, C. Kiyanda, M. Radulescu, J. Lee, K. Bates, and N. Nikiforakis, "Nonlinear dynamics and chaos analysis of one-dimensional pulsating detonations," *Combustion Theory and Modelling*, vol. 9, no. 1, pp. 159–170, 2005.
- [4] A. K. Henrick, T. D. Aslam, and J. M. Powers, "Simulations of pulsating one-dimensional detonations with true fifth order accuracy," *Journal of Computational Physics*, vol. 213, no. 1, pp. 311–329, 2006.
- [5] M. I. Radulescu and J. Tang, "Nonlinear dynamics of self-sustained supersonic reaction waves: Ficketts detonation analogue," *Physical review letters*, vol. 107, no. 16, p. 164503, 2011.
- [6] A. R. Kasimov, L. M. Faria, and R. R. Rosales, "Model for shock wave chaos," *Physical review letters*, vol. 110, no. 10, p. 104104, 2013.
- [7] A. Bellerive and M. I. Radulescu, "Chaos in a Third Order Nonlinear Evolution Equation for Pulsating Detonations using Ficketts Model," in *Proceedings of the 25th ICDERS*, Leeds UK, 2015.
- [8] M. I. Radulescu and J. E. Shepherd, "Dynamics of galloping detonations: Inert hydrodynamics with pulsed energy release," in *Bulletin of the American Physical Society, 68th Annual Meeting of the APS Division of Fluid Dynamics*, Boston, MA, Nov. 2015.
- [9] R. R. Rosales and A. Majda, "Weakly nonlinear detonation waves," *SIAM Journal on Applied Mathematics*, vol. 43, no. 5, pp. 1086–1118, 1983.
- [10] P. Clavin and F. A. Williams, "Dynamics of planar gaseous detonations near Chapman-Jouguet conditions for small heat release," *Combustion Theory and Modelling*, vol. 6, no. 1, pp. 127–139, 2002.
- [11] L. M. Faria, A. R. Kasimov, and R. R. Rosales, "Theory of weakly nonlinear self-sustained detonations," *Journal of Fluid Mechanics*, vol. 784, pp. 163–198, 2015.
- [12] J. Clarke, P. Roe, L. Simmonds, and E. Toro, "Numerical studies of a detonation analogue," *Journal of Energetic Materials*, vol. 7, no. 4-5, pp. 265–296, 1989.
- [13] X. Mi and A. J. Higgins, "Influence of discrete sources on detonation propagation in a Burgers equation analog system," *Physical Review E*, vol. 91, no. 5, p. 053014, 2015.